

S-MUSt3R: Sliding Multi-view 3D Reconstruction

Leonid Antsfeld, Boris Chidlovskii, Yohann Cabon, Vincent Leroy, Jerome Revaud

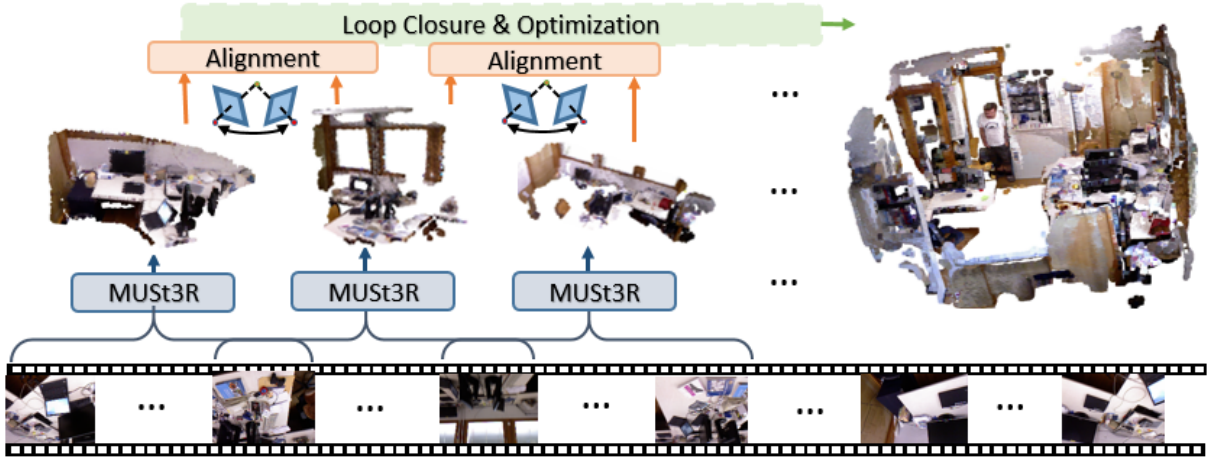


Fig. 1. S-MUSt3R partitions the long image sequence in segments, applies MUSt3R model, then aligns the segments and corrects the accumulated drift with lightweight loop closure and optimization.

Abstract—The recent paradigm shift in 3D vision led to the rise of foundation models with remarkable capabilities in 3D perception from uncalibrated images. However, extending these models to large-scale RGB stream 3D reconstruction remains challenging due to memory limitations. This work proposes S-MUSt3R, a simple and efficient pipeline that extends the limits of foundation models for monocular 3D reconstruction. Our approach addresses the scalability bottleneck of foundation models through a simple strategy of sequence segmentation followed by segment alignment and lightweight loop closure optimization. Without model retraining, we benefit from remarkable 3D reconstruction capacities of MUSt3R model and achieve trajectory and reconstruction performance comparable to traditional methods with more complex architecture. We evaluate S-MUSt3R on TUM, 7-Scenes and proprietary robot navigation datasets and show that S-MUSt3R runs successfully on long RGB sequences and produces accurate and consistent 3D reconstruction. Our results highlight the potential of leveraging the MUSt3R model for scalable monocular 3D scene in real-world settings, with an important advantage of making predictions directly in the metric space.

I. INTRODUCTION

Perceiving three-dimensional environments from monocular RGB streams is a fundamental capability for autonomous systems, yet current methodologies remain limited when applied to long uncalibrated sequences. Existing approaches [10], [46], [48] have demonstrated progress on large-scale monocular scenes, but they frequently rely on multi-component pipelines or presuppose accurate camera intrinsics. Alternative solutions integrate auxiliary sensing modalities such as LiDAR [50], IMU [49], or stereo vision [6], thereby circumventing the core problem of monocular reconstruction. However, scalable

and calibration-free 3D reconstruction from monocular RGB alone remains an open challenge, and addressing it is critical for a broad range of robotic and embodied agent navigation tasks in diverse real-world environments.

A paradigm shift comes from the 3D vision domain which has recently witnessed the rise of feed-forward foundation models based on the Transformer architecture [38]. The seminal work DUSt3R [44] followed by MASt3R [19], MASt3R-SfM [11], CUT3R [43] and FASt3R [45], aim to replace multi-component SfM and SLAM pipelines with a single and unified deep learning network. Trained on massive datasets with backpropagation of errors through the entire pipeline integrating 3D scene representation, camera pose and intrinsic parameter estimation, these models enable robust 3D reconstruction from one or a few uncalibrated RGB images. They predict pointmaps, depths and camera poses in a single forward pass creating powerful foundation models for end-to-end 3D scene understanding.

The most advanced models, such as VGGT [41] and MUSt3R [2], achieve state-of-the-art local reconstructions, but their scalability is constrained by the heavy computational and memory demands of transformer-based architectures. While techniques like Flash-Attention [8] improve efficiency, GPU memory consumption remains high, restricting these models to relatively short sequences. Even high-end GPUs process only a few hundred frames before memory limits are reached, making large-scale reconstructions unfeasible.

To overcome this limitation, recent efforts integrate foundation models into larger systems. One example is MASt3R-

SLAM [25] which combines MAST3R with a complex backend of pose graph optimization and bundle adjustment. In contrast, VGGT-Long [9] adopts a *minimalist* approach, demonstrating that foundation models themselves can serve as a powerful engine for large-scale 3D perception with limited additional overhead.

In a similar spirit, we propose S-MUST3R, a sliding-window extension of MUST3R [2] for long sequences. Our framework partitions input videos into overlapping segments, reconstructs each independently, then aligns and stitches them with a lightweight loop closure module. This approach requires no model retraining, it exploits the strong local accuracy of MUST3R, while it also addresses drift and scalability issues without requiring a sophisticated graph-based optimization backend. The result is a globally consistent 3D reconstruction system that remains simple, efficient, and directly applicable to downstream tasks such as robot navigation [1]. Our choice of MUST3R as the foundation model is guided by its capacity to make predictions directly in the metric space.

Our work makes the following key contributions:

- 1) We extend MUST3R foundation model to large-scale scenes, without requiring camera calibration. We adopt a segment-process-stitch approach that mitigates memory constraints on long sequences.
- 2) We propose multiple improvements which address drift accumulation with lightweight alignment and loop closure, showing that MUST3R can scale without a complex backend.
- 3) We provide extensive quantitative comparisons to state-of-the-art uncalibrated methods and show that S-MUST3R is on par with MAST3R-SLAM and VGGT-SLAM which deploy sophisticated graph-based backends, and outperforms by a large margin the stitching-based competitor method VGGT-Long [9].

II. RELATED WORK

Classical scene reconstruction. Traditional scene reconstruction methods rely on geometric features to estimate camera poses and reconstruct 3D scenes from multi-view images [4], [12], [28]. Using multi-view geometry [18] and bundle adjustment [26], [29], these pipelines extract sparse features, match them, and optimize for SE(3) transformations. Learning-based methods depart from handcrafted SfM [5], [14], [17], [30] and aim to directly predict 3D geometry and camera parameters from one or more RGB images. Neural networks learn strong 3D priors, either object-centric [21], [27] or scene-level [33], [36], [42], [53], often via differentiable SfM trained end-to-end.

Transformer-based feed-forward reconstruction. The seminal work DUST3R [44] introduced feed-forward dense stereo reconstruction from image pairs, producing point maps without requiring known intrinsics. Its successor MAST3R [19] improved pairwise matching with learned descriptors and was later extended to dynamic scenes [51] and multi-image optimization [11]. To move beyond pairwise processing, several works proposed memory or recurrent mechanisms.

Spann3R [40] employed a spatial memory to track observations in sequential pairs. CUT3R [43] used recurrent state modules for incremental multi-view reconstruction, while Pow3R [15] improved robustness by incorporating optional intrinsics, poses, or depth.

MUST3R [2] generalized DUST3R framework to N -view settings with a multi-layer memory for representing scenes as pointmaps, enabling direct image-to-image correspondences, Fast3R [45] replaced pairwise attention with all-to-all attention, VGGT [41] further extended Transformers to output cameras, depths, pointmaps, and tracks, all scaling to hundreds of views in one pass.

SLAM on uncalibrated images. Traditional SLAM systems [3], [23], [24] rely on geometric optimization, while learning-based approaches [16], [37] integrate differentiable components. To exploit 3D foundation models, MAST3R-SLAM [25] built real-time monocular pipelines around MAST3R [19], including efficient transform estimation and loop closure. VGGT-SLAM [22] instead incrementally aligned VGGT submaps through SL(4) optimization, overcoming the limitations of similarity-based alignment.

The closest to ours is VGGT-Long [9] which deploys VGGT [41] as the foundation model for processing sequence segments and SIM(3) groups to align them in one global 3D representation. However, VGGT output is non-metric, and the robot needs additional cues to resolve scale, combine it with stereo, LiDAR or wheel odometry to recover metric scale. Unlike VGGT-Long, S-MUST3R uses MUST3R as the foundation model to process individual segments, it takes advantage from MUST3R producing scene geometry in absolute physical units that can be used on the real robots. The robot can directly use the predictions to estimate traversability, collision avoidance and in path planning.

III. ARCHITECTURE

A. MUST3R

MUST3R [2] extends pair-wise DUST3R to an arbitrary number of images and maps them in 3D pointmaps in a first frame’s coordinate system. It uses a multi-layered memory, which contains patches of previously seen images. To control the memory size growing linearly with the number of images, MUST3R applies a special strategy to carefully select memory tokens using the image discovery rate; it leverages a running memory and updates 3D scene of current observations on-the-fly. For an input image I of size $H \times W$, MUST3R outputs its pointmap $\mathbf{X} \in R^{3 \times H \times W}$, confidence map $\mathbf{C} \in R^{H \times W}$ and depth map $\mathbf{d} \in R^{H \times W}$. MUST3R is able to process hundreds of images, but hits the memory limits on longer sequences. In the next section we complement MUST3R with additional steps of segmenting long input sequences and stitching local 3D pointmaps in the global one. We propose multiple modifications to the aligning, stitching and loop closure in order to ensure a robust 3D reconstruction.

B. S-MUST3R

S-MUST3R is a sliding version of MUST3R running over long monocular image sequences. First, it splits the sequence

into overlapping segments; second, MUSt3R processes segments one by one; third, it aligns the segments to express in the first frame’s reference, correct the final representation by detecting segment-wise loops, building a pose graph where segments are nodes and the edges are constrained by alignments, followed by pose graph optimization. Thus we benefit from local reconstruction of segments by MUSt3R while ensuring global accuracy when fast and efficient collecting segments in the full dense scene pointmap.

An input sequence of N images, $\{I_i\}_{i=1}^N$ is first partitioned into a number of overlapping segments. The generated segments all have the same length l and the overlap size p . The first segment S_1 includes frames from 1 to l , the second segment S_2 includes frames from $l-p+1$ to $2*l-p$, and so on.

C. Confidence weighted by depth difference

MUSt3R trains the model using a confidence-aware loss and predicts a confidence score for each pixel in the images. The segment alignment is sensible to 3D outliers and accurate confidence maps are critical for filtering the outliers out. We therefore take advantage from segment overlaps as an additional source of information for confidence estimation. The same image gets different context in adjacent segments, and MUSt3R model often output different depth estimation for the same image. Any inconsistency in depth estimation can undermine the accurate segment alignment.

To align 3D pointmaps of two overlapping segments we use both confidence and depth maps; we trust points with higher confidence and down-weight points with inconsistent depth. Given confidence values c_{ip}, c_{jp} and depth values d_{ip}, d_{jp} for pixel p of the image I present in overlapping segments S_i and S_j , we modulate the confidences by penalizing the depth disagreement with weight w . This weight

$$w = \frac{c_{ip} \cdot c_{jp}}{1 + |d_{ip} - d_{jp}|} \quad (1)$$

is used to update the confidence values $c'_{ip} = w \cdot c_{ip}$ and $c'_{jp} = w \cdot c_{jp}$. With some abuse of notation, in the following we denote the updated confidence maps as $\mathbf{C}_i, \mathbf{C}_j$.

D. Transform groups

Stitching local pointmaps in the global one relies on the accurate estimation of all segment alignments in order to express all 3D point coordinates in the first frame’s reference. It is common to estimate transforms using SIM(3) Lie group [9], [31], [37] for which there exist close form and fast iterative solutions. However, the rigid transformations defined by SIM(3) group assume that input images are calibrated. In the case of uncalibrated images, it requires relaxation [22] as the rigid transformation can not cope with different distortions in the output of multi-view methods, like stretching and angular deformations of the scene geometry. Recent works propose to replace SIM(3) group with Affine(3) [47] or SL(4) groups [22] to cope with such distortions.

In the following we consider the alignment between two segments as belonging to transform group \mathcal{T} , where \mathcal{T} is

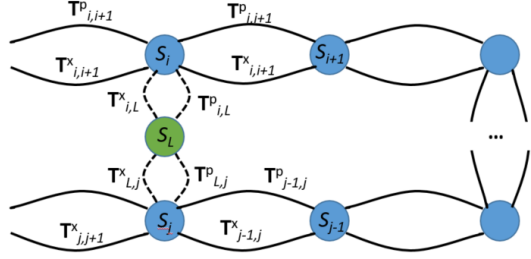


Fig. 2. Example of a pose graph where segments are nodes (nodes in blue for sequence segments and an extra node in green for loop closure) and edges are constrained by pose-driven and pointmap-driven alignments.

one of three Lie groups of increasing complexity, SIM(3), Affine(3) or SL(4). Conventional SIM(3) group includes rotations, translations and uniform scaling. Affine(3) group includes in addition non-uniform scaling and shearing. Then, SL(4) group includes translations, scaling and projective warping. We note however that a higher expressive power comes with a higher compute cost. In Sec. IV, we report the evaluation results and show that SIM(3) represents a globally best performance-speed compromise for our pipeline.

E. Segment Aligning with Confidence and Depth

MUSt3R processes segments independently; given an segment S_k , it outputs a 3D pointmap \mathbf{X}_k , confidence map \mathbf{C}_k , per-frame depth estimation \mathbf{d}_k , completed with segment-wise consistent camera poses \mathbf{p}_k . We leverage MUSt3R’s confidence as well the frame-based depth estimation to robustly align the overlapping segments.

For two adjacent segments, S_k and S_{k+1} , we identify a set of 3D point correspondences $(\mathbf{X}_k^i, \mathbf{X}_{k+1}^i)$ and confidences $(\mathbf{C}_k^i, \mathbf{C}_{k+1}^i)$ within their overlapping region. To robustly estimate the transformation $\mathbf{T}_{k,k+1} \in \mathcal{T}$ that aligns S_{k+1} to S_k , we deploy, in the case of SIM(3) and Affine(3) transforms, the Iteratively Reweighted Least Squares (IRLS) optimization [9]. Its objective is to minimize the following robust cost function

$$\mathbf{T}_{k,k+1}^x = \arg \min_{\mathbf{T} \in \mathcal{T}} \sum_i \rho \left(\|\mathbf{X}_k^i - \mathbf{T} \mathbf{X}_{k+1}^i\|_2 \right), \quad (2)$$

where $\rho(\cdot)$ is the Huber loss function which down-weights the influence of outliers. The IRLS procedure solves this non-linear problem by iteratively minimizing a weighted sum of squared errors. We refer to [9] for more detail.

In addition to aligning adjacent segments by 3D correspondences, we propose to align segments S_k and S_{k+1} by another MUSt3R’s output, namely the camera poses $(\mathbf{p}_k^i, \mathbf{p}_{k+1}^i)$, within the overlapping region. In Eq.(2), we replace the pointmap \mathbf{X}_i^j by the set of estimated camera poses \mathbf{p}_i^j . Due to a much smaller size, the inference of the alignment from camera poses is negligible w.r.t. pointmaps,

$$\mathbf{T}_{k,k+1}^p = \arg \min_{\mathbf{T} \in \mathcal{T}} \sum_i \rho \left(\|\mathbf{P}_k^i - \mathbf{T} \mathbf{P}_{k+1}^i\|_2 \right). \quad (3)$$

Therefore, for two adjacent segments S_k and S_{k+1} we obtain two transform estimations, $\mathbf{T}_{k,k+1}^x$ and $\mathbf{T}_{k,k+1}^p$, inferred from

pointmaps and camera poses, respectively. In the pose graph, they form two edges connecting nodes S_k and S_{k+1} (blue nodes in Fig. 2).

Unlike $\text{SIM}(3)$ and $\text{Affine}(3)$ groups, aligning segments with transforms from $\text{SL}(4)$ group requires estimating a relative homography matrix between the segments; we use h-solver from VGGT-SLAM [22].

F. Loop Detection and Global Optimization

Long sequences result in the drift accumulation. We remove the drift by detecting and closing loops across the entire sequence. This process involves finding visual content shared by non-adjacent segments and robustly estimating the transform $\mathbf{T} \in \mathcal{T}$ between them.

First, we reuse output of MUSt3R’s encoder which generates patch features for any image I in the sequence. They are average-pooled to obtain a compact global feature vector \mathbf{f} which captures the scene geometry in the image. These global image descriptors are used to identify potential loop closure candidates. We create and maintain KDTree() structure D of image descriptors; and for each descriptor, we perform an efficient nearest neighbor search in D to find other images with high similarity. A pair of distant images $(I, I'), I \in \mathcal{S}_i, I' \in \mathcal{S}_j, |i - j| > 2$ forms a potential loop closure if their similarity score exceeds a threshold σ_{sim} . Two distant segments with at least $k_{min} = 3$ loop closure candidates form a loop.

For validated loop pairs (I, I') , we generate an additional reconstruction of the scene location where the loop occurs. We form a new segment \mathcal{S}_L by concatenating images surrounding images $I \in \mathcal{S}_i$ and images $I' \in \mathcal{S}_j$. This segment \mathcal{S}_L contains distant views of the same scene location and overlaps with segments \mathcal{S}_i and \mathcal{S}_j . Processed by MUSt3R model, this additional local reconstruction complements the sequential processing of adjacent segments and provides S-MUSt3R with a more diverse, time-dispersed perspective, enabling a more robust scene reconstruction.

The 3D pointmap of segment \mathcal{S}_L is then aligned with the pointmaps of the corresponding segments \mathcal{S}_i and \mathcal{S}_j . We close the loop in the pose graph by chaining the alignments through the new segment \mathcal{S}_L (see green node in Fig. 2). We compute transforms to align segment \mathcal{S}_i and segment \mathcal{S}_L , then \mathcal{S}_L and \mathcal{S}_j . Similarly to the processing of adjacent segments, we complete the pose graph with two transforms, $\mathbf{T}_{i,L}^x$ and $\mathbf{T}_{i,L}^p$, which align \mathcal{S}_i and \mathcal{S}_L , and two transforms, $\mathbf{T}_{L,j}^x$ and $\mathbf{T}_{L,j}^p$ which align \mathcal{S}_L and \mathcal{S}_j . They provide additional geometric constraints for the global optimization by bridging the two distant segments through an additional local 3D reconstruction.

Once the graph is completed, we can globally optimize all transforms in the pose graph [10], [20]. The pose graph is composed of adjacent and loop segments; built segment-wise, it is much smaller in the number of nodes and edges than complex frame-based factor graphs constructed by MAST3R-SLAM and VGGT-SLAM. We minimize an objective function composed of two types of geometric constraints: sequential

constraints from adjacent segments (Sec. III-E) and loop closure constraints from non-adjacent segments.

This non-linear least-squares problem is efficiently solved using the Levenberg-Marquardt (LM) algorithm. By blending Gauss-Newton with gradient descent, the LM algorithm redistributes error over all nodes so that all constraints are satisfied as much as possible. It operates segment-wise and converges in few iterations, due to a small graph size.

IV. EXPERIMENTS

We evaluate S-MUSt3R on standard RGB SLAM benchmarks to assess the camera pose and angle estimation accuracies on the 7-Scenes [32] and TUM RGB-D [34] datasets; we report root mean square error (RMSE) of the absolute pose error (APE) using EVO metric [13]. We also evaluate the 3D reconstruction on a proprietary dataset of uncalibrated image sequences collected by navigational robots in a multi-room office environment. On 7-Scenes and TUM RGB-D datasets, we compare S-MUSt3R with the state-of-the-art approaches in uncalibrated setting: DROID-SLAM [37], MAST3R-SLAM [25], VGGT-SLAM [22] and VGGT-Long [9]. We use reported numbers from MAST3R-SLAM [25] and VGGT-SLAM [22] for baselines, including the uncalibrated version of DROID-SLAM which estimates intrinsics with an automatic calibration pipeline [39]. For the sake of comparison, we also include the state-of-the-art methods for the calibrated setting [3], [7], [20], [52], [35], [54] provided with camera intrinsics.

We use the MUSt3R_512.pth pre-trained model with ViT-L encoder and ViT-B decoder available at <https://github.com/naver/must3r>. For the fair comparison with the competitor VGGT-Long, we run S-MUSt3R with the segment length $l=60$ and overlap $p=30$, and $\text{SIM}(3)$ transform group. The cosine similarity threshold is $\sigma_{sim} = 0.95$. In ablation studies (Sec. IV-B), we run S-MUSt3R with other segmentation parameters and transform groups.

A. Pose estimation evaluation

As shown in Tabs. I and II, S-MUSt3R performs comparably to the top performing uncalibrated baselines on 7-Scenes and TUM RGB-D datasets. On 7-Scenes, S-MUSt3R shows the same APE as the top performing baselines MAST3R-SLAM and VGGT-SLAM, despite the lightweight loop closure and global optimization. On the TUM dataset, S-MUSt3R performs the best overall with an average error of 0.052 m. At the same time, it outperforms by a large margin the competitor VGGT-Long on all sequences of the two datasets, under the same segmentation strategy. This demonstrates that we are able to extend MUSt3R to multiple sequences with a rather simple pipeline of segmenting the input sequence and stitching local pointmaps.

In addition to the camera pose estimation with APE, we estimate the average angular error (AAE) and compare S-MUSt3R to VGGT-Long on more complex *freiburg2* and *freiburg3* TUM scenes. As Tab. III shows, S-MUSt3R generates more accurate estimation with the lower pose and

TABLE I

ROOT MEAN SQUARE ERROR (RMSE) OF ABSOLUTE POSE ERROR (APE) ON TUM RGB-D [34]. THE GRAY ROWS INDICATE THE RESULTS USING THE CALIBRATED CAMERA INTRINSICS; SYMBOL '*' INDICATES BASELINES EVALUATED IN THE UNCALIBRATED MODE. GREEN IS BEST AND LIGHT GREEN ARE SECOND AND THIRD BEST.

	Method	sequence										Avg
		360	desk	desk2	floor	plant	room	rpy	teddy	xyz		
Calibr.	ORB-SLAM3 [3]	×	0.017	0.210	×	0.034	×	×	×	0.009	N/A	
	DeepV2D [35]	0.243	0.166	0.379	1.653	0.203	0.246	0.105	0.316	0.064	0.375	
	DeepFactors [7]	0.159	0.170	0.253	0.169	0.305	0.364	0.043	0.601	0.035	0.233	
	DPV-SLAM [20]	0.112	0.018	0.029	0.057	0.021	0.330	0.030	0.084	0.010	0.076	
	DPV-SLAM++ [20]	0.132	0.018	0.029	0.050	0.022	0.096	0.032	0.098	0.010	0.054	
	GO-SLAM [52]	0.089	0.016	0.028	0.025	0.026	0.052	0.019	0.048	0.010	0.035	
	DROID-SLAM [37]	0.111	0.018	0.042	0.021	0.016	0.049	0.026	0.048	0.012	0.038	
Uncalibr.	MAS3R-SLAM [25]	0.049	0.016	0.024	0.025	0.020	0.061	0.027	0.041	0.009	0.030	
	DROID-SLAM* [37]	0.202	0.032	0.091	0.064	0.045	0.918	0.056	0.045	0.012	0.158	
	MAS3R-SLAM* [25]	0.070	0.035	0.055	0.056	0.035	0.118	0.041	0.114	0.020	0.060	
	VGGT-SLAM, SIM(3) [22]	0.123	0.040	0.055	0.254	0.022	0.088	0.041	0.032	0.016	0.074	
	VGGT-SLAM, SL(4) [22]	0.071	0.025	0.040	0.141	0.023	0.102	0.030	0.034	0.014	0.053	
	VGGT-Long [9]	0.063	0.059	0.045	0.108	0.057	0.172	0.056	0.137	0.051	0.083	
	S-MUSt3R(ours)	0.062	0.031	0.047	0.054	0.054	0.065	0.028	0.115	0.018	0.052	

TABLE II

ROOT MEAN SQUARE ERROR (RMSE) OF ABSOLUTE TRAJECTORY ERROR (ATE) ON 7-SCENES [32] (UNIT: M).

	Method	Sequence							Avg
		chess	fire	heads	office	pumpkin	kitchen	stairs	
Calibr.	NICER-SLAM [54]	0.033	0.069	0.042	0.108	0.200	0.039	0.108	0.086
	DROID-SLAM [37]	0.036	0.027	0.025	0.066	0.127	0.040	0.026	0.049
	MAS3R-SLAM [25]	0.053	0.025	0.015	0.097	0.088	0.041	0.011	0.047
Uncalibr.	DROID-SLAM* [37]	0.047	0.038	0.034	0.136	0.166	0.080	0.044	0.078
	MAS3R-SLAM* [25]	0.063	0.046	0.029	0.103	0.114	0.074	0.032	0.066
	VGGT-SLAM, SIM(3) [22]	0.037	0.026	0.018	0.104	0.133	0.061	0.093	0.067
	VGGT-SLAM, SL(4) [22]	0.036	0.028	0.018	0.103	0.133	0.058	0.093	0.067
	VGGT-Long [9]	0.054	0.055	0.059	0.110	0.245	0.067	0.055	0.092
	S-MUSt3R(ours)	0.054	0.041	0.028	0.098	0.145	0.053	0.057	0.067

angular errors than VGGT-Long, in the same segmentation setup (segment length $l=60$ and overlap $p=30$).

Finally, we run MAS3R-SLAM, MUSt3R, VGGT-Long and S-MUSt3R on the robot navigation collection. As Tab. IV shows, the first three methods work well except when robots navigate in a narrow corridor with featureless walls (see at the bottom of Fig. 5) while S-MUSt3R allows to recover the robot track thanks to segment overlaps and loop closures.

B. Ablations

We report ablation studies performed on S-MUSt3R pipeline with conclusions summarized as follows: (a) the effect of different values of segment length l , where cutting the input sequence in longer sequences leads generally to higher accuracy on 3D reconstruction and pose estimation, (b) comparison of three transform groups, where SIM(3) transform group represents a globally more reliable solution for aligning segments than Affine(3) and SL(4), (c) the effect of loop closure and global optimization which leads to reducing the pose and angular errors, and estimating both alignments between two overlapping segments, using pointmaps \mathbf{T}_{ij}^x and camera poses \mathbf{T}_{ij}^p , is the winner strategy.

Segment length. Tab. V ablates the segment length for two sequences from 7-Scenes and TUM, with the segment size l varying from 20 to 200 and the overlap p fixed to $l/2$. In both

sequences, partitioning the input sequence in longer segments and stitching fewer local pointmaps help to reduce both average angular and pose errors. They provide a substantial gain over the default case $l = 60$ and bring S-MUSt3R closer to the results achieved of MUSt3R that processes the full sequence in one pass.

Transform groups. All S-MUSt3R results in Tabs. I and II are reported using SIM(3) as the transformation group. We additionally evaluated our pipeline with two alternative groups: Affine(3) and SL(4). Across all experiments, SIM(3) consistently demonstrated its strength by delivering fast and reliable estimates of both pointmaps and camera poses. Substituting SIM(3) with the more expressive Affine(3) group led to only a modest improvement, reducing APE by about 0.5%. In contrast, the SL(4) group showed mixed performance: while it achieved up to a 4% APE reduction in three sequences, it failed to produce stable alignments in two others, requiring additional per-scene parameter tuning. These results confirm the sensibility of SL(4) to outliers and its tendency toward unstable homographic solutions in the presence of planar structures, an issue also noted in [22].

Another key consideration is computation time. For short segments, transform estimation times are comparable across all groups. However, once the segment length l exceeds 100, the cost for Affine(3) and especially SL(4) increases

TABLE III

AVERAGE POSE AND ANGULAR ERRORS OF VGGT-LONG AND S-MUST3R, ON FREIBURG2 AND FREIBURG3 TUM SCENES. GREEN IS THE BEST.

Method	Error	cabi net	large cabinet	long.off house	nostr tex_far	nostrtex near_wl	sitting half	sitting rpy	sitting stat	walking xyz	teddy
VGGT-Long [9]	APE	0.095	0.127	0.167	0.156	0.154	0.211	0.061	0.014	0.169	0.170
	AAE	3.319	4.913	5.60	7.97	2.25	19.87	93.48	12.71	15.35	5.575
S-MUST3R(ours)	APE	0.072	0.109	0.081	0.091	0.243	0.136	0.054	0.012	0.158	0.054
	AAE	7.41	2.92	2.48	22.77	11.38	10.35	84.64	16.97	13.04	5.335

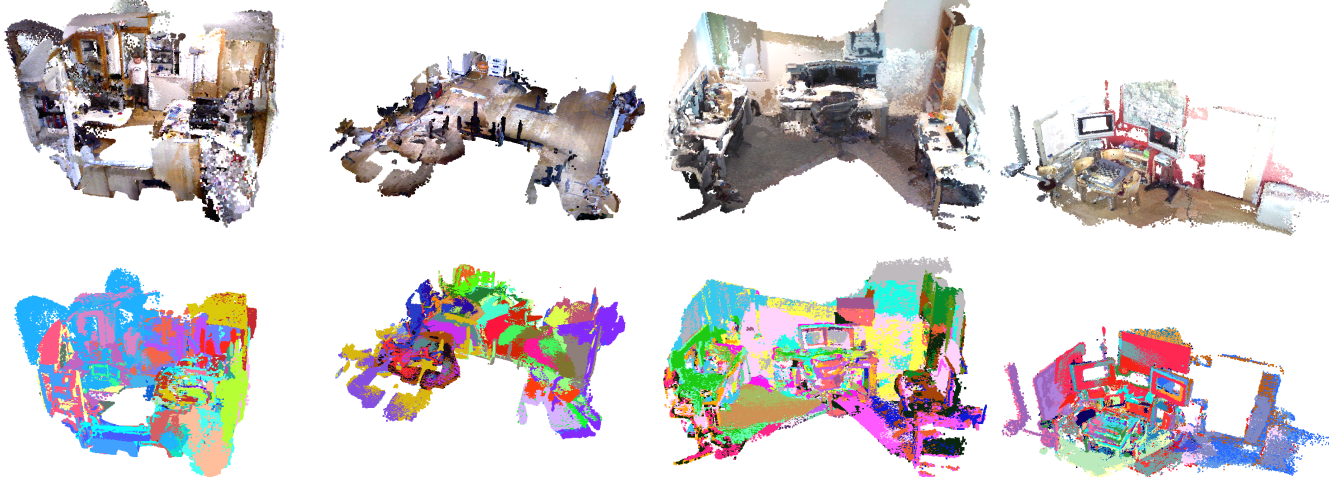


Fig. 3. 3D reconstruction with S-MUST3R for room and floor sequences of TUM dataset and office and chess of 7-Scenes dataset. Top: 3D reconstruction with original RGB colors; Bottom: segment pointmaps shown with different colors.

TABLE IV

AVERAGE POSE AND ANGULAR ERRORS ON ROBOT NAVIGATION COLLECTION

Method	AAE	APE
MAS3R-SLAM [25]	29.47	1.580
MUST3R [2]	11.87	1.871
VGGT-Long [9]	33.31	2.239
S-MUST3R (ours)	7.10	0.251

TABLE V

ABLATION ON SEGMENT LENGTH: AAE AND APE FOR TUM AND 7-SCENES. GREEN IS THE BEST, YELLOW REFERS TO TABS. I AND II.

Method	TUM teddy		7-Scenes pumpkin	
	AAE	APE	AAE	APE
S-MUST3R $l=20$	9.59	0.185	3.88	0.156
S-MUST3R $l=40$	8.30	0.164	3.92	0.155
S-MUST3R $l=60$	7.66	0.115	3.77	0.145
S-MUST3R $l=80$	4.78	0.091	3.83	0.146
S-MUST3R $l=100$	6.03	0.141	3.13	0.147
S-MUST3R $l=200$	4.27	0.087	4.12	0.141
MUST3R [2]	1.42	0.061	3.36	0.137

rapidly. As a result, S-MUST3R is forced to heavily sparsify the pointmaps on longer segments before applying SL(4) transforms, effectively negating the potential benefits of a more expressive transformation group. Overall, within our pipeline, SIM(3) proves to be the most reliable and balanced choice among the three.

Metric vs non-metric predictions. As mentioned before, S-MUST3R inherits the accurate metric output from MUST3R. Error of scale estimation of S-MUST3R is less than 2% on

both TUM and 7-Scenes. This makes predictions directly deployable for the robot navigation, while VGGT-Long predictions require other sources of information for rescaling before acting in robot navigation. In Tabs. I and II results for both VGGT-Long and S-MUST3R are reported after rescaling.

Loop closure and global optimization. Despite the lightweight segment-wise approach, the loop closure and optimization reduces APE and AAE. The average gain on 7-Scenes is 14% and 3%, respectively. Fig. 4 shows trajectory of TUM and 7-Scenes sequences, before and after optimization. Moreover, estimating two alignments, from pointmaps and camera poses, is beneficial; dropping the former reduces the gain by 4% and the latter by 3%.

C. Qualitative results

In this section, we present qualitative results to illustrate the quality of scene reconstruction by S-MUST3R.

Fig. 4 (top) shows examples of 3D scene reconstruction with original RGB colors of floor and desk scenes from TUM RGB-D dataset, and office and chess from 7-Scenes. Additionally, Fig. 3 (bottom) shows the same scenes with all segments painted with different colors; this help to visualize the alignments between segments and contribution of each segment in the final scene reconstruction.

Fig. 4 demonstrates the effect of using lightweight loop closure optimization on correcting segment poses in TUM and 7-Scenes datasets.

Fig. 5 illustrates scene reconstruction from a robot navigation sequence. Figs. 5(left) and (middle) show the pointmap generated by S-MUST3R with the estimated robot trajectory

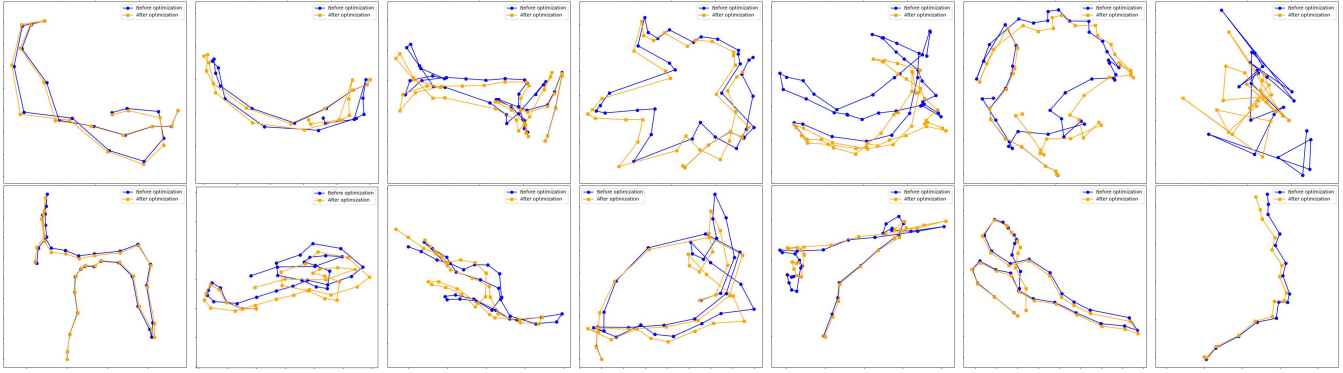


Fig. 4. Segment pose correction with lightweight loop closure, for TUM (top) and 7-Scenes (down) datasets.

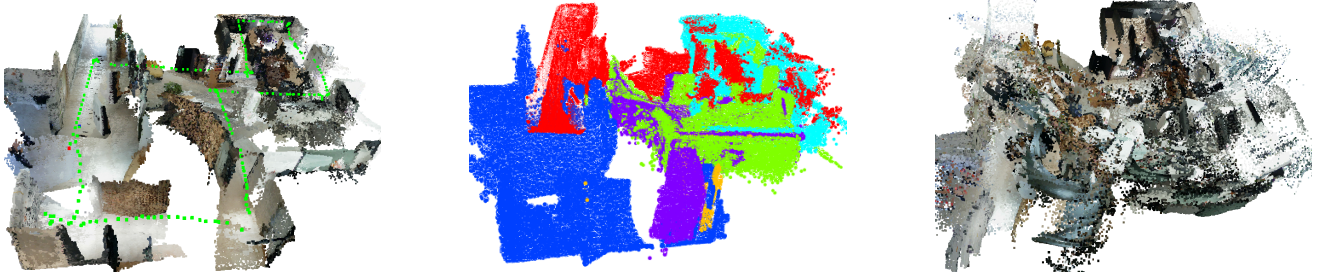


Fig. 5. 3D reconstruction from a robot navigation sequence with S-MUSt3R in RGB (left) and segment-colored (middle) versions and with VGGT-Long (right).

and its segment-colored version. Instead, the scene reconstruction with VGGT-Long in Fig. 5(right) is much less accurate. For better visualization, both 3D representations have been modified by removing the ceiling of the scene.

D. Limitations

A clear limitation of the stitching approach is its strong dependence on the quality of local reconstructions produced by the foundation model. While S-MUSt3R shows some ability to mitigate these errors, by leveraging segment overlaps as an additional source of information to filter out inaccuracies from the MUSt3R model, this effect remains limited in scope.

Another limitation, shared with most SLAM methods that rely on loop closure to correct drift, is the high sensitivity to hyperparameters such as the similarity threshold σ_{sim} . More robust alternatives, including self-tuning mechanisms, adaptive acceptance thresholds, or probabilistic formulations, could be integrated to improve outlier detection and enhance the reliability of loop closure.

V. CONCLUSIONS

In this paper, we introduce S-MUSt3R, a simple yet effective pipeline that extends the capabilities of the MUSt3R foundation model for monocular 3D reconstruction from uncalibrated images. The method tackles scalability by segmenting input sequences, aligning the resulting segments, and applying lightweight loop closure optimization. Several design improvements are incorporated to enhance accuracy and consistency, yielding more robust alignments and reconstructions. Experiments on the 7-Scenes, TUM and robot navigation datasets demonstrate that S-MUSt3R achieves consistent 3D

reconstructions from long RGB sequences. These results underline the potential of leveraging the MUSt3R model for scalable monocular 3D scene reconstruction in real-world scenarios, with the key advantage of producing predictions directly in metric space.

REFERENCES

- [1] Dhruv Batra, Aaron Gokaslan, Ani Kembhavi, Oleksandr Maksymets, Roozbeh Mottaghi, Manolis Savva, Alexander Toshev, and Erik Wijmans. ObjectNav Revisited: On Evaluation of Embodied Agents Navigating to Objects. *CoRR*, 2006.13171, 2020.
- [2] Johann Cabon, Lucas Stoffl, Leonid Antsfeld, Gabriela Csurka, Boris Chidlovskii, Jérôme Revaud, and Vincent Leroy. MUSt3R: Multi-view Network for Stereo 3D Reconstruction. In *Proceedings of the Computer Vision and Pattern Recognition Conference*, pages 1050–1060. Computer Vision Foundation / IEEE, 2025.
- [3] Carlos Campos, Richard Elvira, Juan J. Gomez Rodriguez, Jose M. M. Montiel, and Juan D. Tardos. ORB-SLAM3: An accurate open-source library for visual, visual-inertial, and multimap SLAM. *IEEE Transactions on Robotics*, 37(6):1874–1890, dec 2021.
- [4] Andrei Cramariuc, Lukas Bernreiter, Florian Tschopp, Marius Fehr, Victor Reijgwart, Juan Nieto, Roland Siegwart, and Cesar Cadena. maplab 2.0–A Modular and Multi-Modal Mapping Framework. *IEEE Robotics and Automation Letters*, 8(2):520–527, 2022.
- [5] David Crandall, Andrew Owens, Noah Snavely, and Dan Huttenlocher. SfM with MRFs: Discrete-Continuous Optimization for Large-Scale Structure from Motion. *IEEE Transactions on Pattern Analysis and Machine Intelligence*, 35(12):2841–2853, 2013.
- [6] Igor Cvišić, Ivan Marković, and Ivan Petrović. Soft2: Stereo visual odometry for road vehicles based on a point-to-epipolar-line metric. *IEEE Transactions on Robotics*, 39(1):273–288, 2022.
- [7] J. Czarnowski, T. Laidlow, R. Clark, and A. Davison. DeepFactors: Real-time probabilistic dense monocular SLAM. *IEEE Robotics and Automation Letters*, 5(2):721–728, 2020.
- [8] Tri Dao. FlashAttention-2: Faster attention with better parallelism and work partitioning. In *International Conference on Learning Representations (ICLR)*, 2024.

[9] Kai Deng, Zexin Ti, Jiawei Xu, Jian Yang, and Jin Xie. Vggt-long: Chunk it, loop it, align it – pushing vggt’s limits on kilometer-scale long rgb sequences. *arXiv preprint arXiv:2507.16443*, 2025.

[10] Kai Deng, Yigong Zhang, Jian Yang, and Jin Xie. Gigaslam: Large-scale monocular slam with hierarchical gaussian splats. *arXiv preprint arXiv:2503.08071*, 2025.

[11] Bardienus Duisterhof, Lojze Zust, Philippe Weinzaepfel, Vincent Leroy, Yohann Cabon, and Jerome Revaud. Mast3r-sfm: a fully-integrated solution for unconstrained structure-from-motion. In *IEEE International Conference on 3D Vision (3DV)*, 2025.

[12] Y. Furukawa, B. Curless, S. M. Seitz, and R. Szeliski. Towards internet-scale multi-view stereo. In *IEEE Conf. on Computer Vision and Pattern Recognition (CVPR)*, pages 1434–1441, 2010.

[13] Michael Grupp. evo: Python package for the evaluation of odometry and SLAM. [urlhttps://github.com/MichaelGrupp/evo](https://github.com/MichaelGrupp/evo), 2017.

[14] Richard Hartley and Andrew Zisserman. *Multiple View Geometry in Computer Vision*. Cambridge University Press, 2004.

[15] Wonbong Jang, Philippe Weinzaepfel, Vincent Leroy, Lourdes Agapito, and Jerome Revaud. Pow3R: Empowering Unconstrained 3D Reconstruction with Camera and Scene Priors. *arXiv preprint arXiv:2503.17316*, 2025.

[16] Krishna Murthy Jatavallabhula, Soroush Saryazdi, Ganesh Iyer, and Liam Paull. gradslam: Automagically differentiable slam. *arXiv preprint arXiv:1910.10672*, 2019.

[17] Nianjuan Jiang, Zhaopeng Cui, and Ping Tan. A Global Linear Method for Camera Pose Registration. In *Proceedings of the International Conference on Computer Vision*, 2013.

[18] J. J. Koenderink and A. J. van Doorn. Affine structure from motion. *Journal of the Optical Society of America A*, 8(2):377–385, 1991.

[19] Vincent Leroy, Yohann Cabon, and Jérôme Revaud. Grounding Image Matching in 3D with MAS3R. In *European Conference on Computer Vision*, 2024.

[20] Lahav Lipson, Zachary Teed, and Jia Deng. Deep patch visual slam. In *European Conference on Computer Vision*, pages 424–440, 2024.

[21] Ruoshi Liu, Rundi Wu, Basile Van Hoorick, Pavel Tokmakov, Sergey Zakharov, and Carl Vondrick. Zero-1-to-3: Zero-shot One Image to 3D Object. In *Proceedings of the Computer Vision and Pattern Recognition Conference*, 2023.

[22] Dominic Maggio, Hyungtae Lim, and Luca Carlone. Vggt-slam: Dense rgb slam optimized on the $sl(4)$ manifold. *arXiv preprint arXiv:2505.12549*, 2025.

[23] Raul Mur-Artal, J. M. M. Montiel, and Juan D. Tardos. ORB-SLAM: A versatile and accurate monocular SLAM system. *IEEE Transactions on Robotics*, 31(5):1147–1163, oct 2015.

[24] Raul Mur-Artal and Juan D. Tardos. ORB-SLAM2: An open-source SLAM system for monocular, stereo, and RGB-d cameras. *IEEE Transactions on Robotics*, 33(5):1255–1262, oct 2017.

[25] Riku Murai, Eric Dexheimer, and Andrew J Davison. Mast3r-slam: Real-time dense slam with 3d reconstruction priors. In *Proceedings of the Computer Vision and Pattern Recognition Conference*, pages 16695–16705, 2025.

[26] Linfei Pan, Daniel Barath, Marc Pollefeys, and Johannes Lutz Schönberger. Global Structure-from-Motion Revisited. In *European Conf. on Computer Vision (ECCV)*, 2024.

[27] Dario Pavlo, David Joseph Tan, Marie-Julie Rakotosaona, and Federico Tombari. Shape, Pose, and Appearance from a Single Image via Bootstrapped Radiance Field Inversion. In *Proceedings of the Computer Vision and Pattern Recognition Conference*, 2023.

[28] A. Rosinol, M. Abate, Y. Chang, and L. Carlone. Kimera: An open-source library for real-time metric-semantic localization and mapping. In *IEEE Intl. Conf. on Robotics and Automation (ICRA)*, pages 1689–1696, 2020. arXiv preprint: 1910.02490.

[29] Johannes L. Schönberger and Jan-Michael Frahm. Structure-from-motion revisited. In *IEEE Conf. on Computer Vision and Pattern Recognition (CVPR)*, pages 4104–4113, 2016.

[30] Johannes Lutz Schönberger and Jan-Michael Frahm. Structure-from-motion revisited. In *Proceedings of the Computer Vision and Pattern Recognition Conference*, 2016.

[31] Thomas Schöps, Torsten Sattler, and Marc Pollefeys. BAD SLAM: Bundle Adjusted Direct RGB-D SLAM. In *Proceedings of the Computer Vision and Pattern Recognition Conference*, 2019.

[32] J. Shotton, B. Glocker, C. Zach, S. Izadi, A. Criminisi, and A. Fitzgibbon. Scene coordinate regression forests for camera relocalization in RGB-D images. In *IEEE Conf. on Computer Vision and Pattern Recognition (CVPR)*, pages 2930–2937, 2013.

[33] Cameron Smith, David Charatan, Ayush Tewari, and Vincent Sitzmann. FlowMap: High-Quality Camera Poses, Intrinsic, and Depth via Gradient Descent. In *3DV*, 2025.

[34] Jürgen Sturm, Nikolas Engelhard, Felix Endres, Wolfram Burgard, and Daniel Cremers. A benchmark for the evaluation of RGB-D SLAM systems. In *IEEE/RSJ Intl. Conf. on Intelligent Robots and Systems (IROS)*, pages 573–580. IEEE, 2012.

[35] Zachary Teed and Jia Deng. DEEPV2D: Video to Depth with Differentiable Structure from Motion. In *Intl. Conf. on Learning Representations (ICLR)*, 2018.

[36] Zachary Teed and Jia Deng. DeepV2D: Video to Depth with Differentiable Structure from Motion. In *ICLR*, 2020.

[37] Zachary Teed and Jia Deng. DROID-SLAM: Deep visual SLAM for monocular, stereo, and RGB-D cameras. In *Advances in Neural Information Processing Systems (NIPS)*, 2021.

[38] Ashish Vaswani, Noam Shazeer, Niki Parmar, Jakob Uszkoreit, Llion Jones, Aidan N Gomez, Łukasz Kaiser, and Illia Polosukhin. Attention is all you need. *Advances in neural information processing systems*, 30, 2017.

[39] Alexander Veicht, Paul-Edouard Sarlin, Philipp Lindenberger, and Marc Pollefeys. GeoCalib: Learning Single-Image Calibration with Geometric Optimization. In *European Conf. on Computer Vision (ECCV)*, pages 1–20. Springer, 2024.

[40] Hengyi Wang and Lourdes Agapito. 3D Reconstruction with Spatial Memory. *arXiv:2408.16061*, 2024.

[41] Jianyuan Wang, Minghao Chen, Nikita Karaev, Andrea Vedaldi, Christian Rupprecht, and David Novotny. Vggt: Visual geometry grounded transformer. In *Proceedings of the Computer Vision and Pattern Recognition Conference*, pages 5294–5306, 2025.

[42] Jianyuan Wang, Nikita Karaev, Christian Rupprecht, and David Novotny. Visual Geometry Grounded Deep Structure From Motion. In *Proceedings of the Computer Vision and Pattern Recognition Conference*, 2024.

[43] Qianqian Wang, Yifei Zhang, Aleksander Holynski, Alexei A Efros, and Angjoo Kanazawa. Continuous 3d perception model with persistent state. *arXiv preprint arXiv:2501.12387*, 2025.

[44] Shuzhe Wang, Vincent Leroy, Yohann Cabon, Boris Chidlovskii, and Jerome Revaud. Dust3r: Geometric 3d vision made easy. In *Conference on Computer Vision and Pattern Recognition*, 2024.

[45] Jianing Yang, Alexander Sax, Kevin J. Liang, Mikael Henaff, Hao Tang, Ang Cao, Joyce Chai, Franziska Meier, and Matt Feiszli. Fast3r: Towards 3d reconstruction of 1000+ images in one forward pass. In *Proceedings of the Computer Vision and Pattern Recognition Conference*, pages 21924–21935, 2025.

[46] Nan Yang, Rui Wang, Jorg Stuckler, and Daniel Cremers. Deep virtual stereo odometry: Leveraging deep depth prediction for monocular direct sparse odometry. In *Proceedings of the European conference on computer vision (ECCV)*, pages 817–833, 2018.

[47] Yifan Yu, Shaohui Liu, Rémi Pautrat, Marc Pollefeys, and Viktor Larsson. Relative pose estimation through affine corrections of monocular depth priors. *arXiv preprint arXiv:2501.05446*, 2025.

[48] Huangying Zhan, Chamara Saro Weerasekera, Jia-Wang Bian, Ravi Garg, and Ian Reid. Df-vo: What should be learnt for visual odometry? *arXiv preprint arXiv:2103.00933*, 2021.

[49] Ji Zhang and Sanjiv Singh. Visual-lidar odometry and mapping: Low-drift, robust, and fast. In *2015 IEEE international conference on robotics and automation (ICRA)*, pages 2174–2181. IEEE, 2015.

[50] Ji Zhang, Sanjiv Singh, et al. Loam: Lidar odometry and mapping in real-time. *2(9):1–9*, 2014.

[51] Junyi Zhang, Charles Herrmann, Junhwa Hur, Varun Jampani, Trevor Darrell, Forrester Cole, Deqing Sun, and Ming-Hsuan Yang. MonST3R: A Simple Approach for Estimating Geometry in the Presence of Motion. *arXiv:2410.03825*, 2024.

[52] Youmin Zhang, Fabio Tosi, Stefano Mattoccia, and Matteo Poggi. GO-SLAM: Global Optimization for Consistent 3D Instant Reconstruction. In *Proceedings of the International Conference on Computer Vision*, pages 3727–3737, 2023.

[53] Huizhong Zhou, Benjamin Ummenhofer, and Thomas Brox. DeepTAM: Deep Tracking and Mapping with Convolutional Neural Networks. *International Journal of Computer Vision*, 128(3):756–769, 2020.

[54] Zihan Zhu, Songyou Peng, Viktor Larsson, Zhaopeng Cui, Martin R Oswald, Andreas Geiger, and Marc Pollefeys. NICER-SLAM: Neural Implicit Scene Encoding for RGB SLAM. In *IEEE International Conference on 3D Vision (3DV)*, pages 42–52, 2024.